Creation of economical and robust large area MCPs by ALD method for photodetectors

Anil U. Mane*[a], Jeffrey W. Elam[a], Wagner G. Robert[a], Oswald H. W. Siegmund[b], Michael J. Minot[c]
[a]Argonne National Laboratory, Lemont, IL USA 60439;
[b]University of California, Berkeley, CA USA 94720;
[c]Incom, Inc, Charlton, MA USA 01507.

ABSTRACT

We report a cost-effective and production achievable path to fabricate robust large-area microchannel plates (MCPs), which offers the new prospect for larger area MCP-based detector technologies. We used atomic Layer Deposition (ALD), a thin film growth technique, to independently adjust the desired electrical resistance and secondary electron emission (SEE) properties of low cost borosilicate glass micro-capillary arrays (MCAs). These capabilities allow a separation of the substrate material properties from the signal amplification properties. This methodology enables the functionalization of microporous, highly insulating MCA substrates to produce sturdy, large format MCPs with unique properties such as high gain (>10^7/MCP pair), low background noise, ~10ps time resolution, sub-micron spatial resolution and excellent stability after only a short (2-3days) scrubbing time.

The ALD self-limiting growth mechanism allows atomic level control over the thickness and composition of resistive and secondary electron emission (SEE) layers that can be deposited conformally on high aspect ratio (~100) capillary glass arrays. We have developed several robust and consistent production doable ALD processes for the resistive coatings and SEE layers to give us precise control over the MCP parameters. Further, the adjustment of MCPs resistance by tailoring the ALD material composition permits the use of these MCPs at high or low temperature detector applications. Here we discuss ALD method for MCP functionalization and a variety of MCP testing results.

Keywords: ALD, microchannel plate, photodetectors, SEE, thin film, psec time resolution, electron amplifier

1. INTRODUCTION

1.1 MCP Applications

High performance photodetectors provide the essential functionality for particle, nuclear and accelerator physics experiments in a wide variety of contexts. Light can be generated by particle cascades in calorimeters, by scintillation in liquid noble gas detectors, in gas avalanches, by Cerenkov radiation in liquid, Cerenkov light in crystals, in extensive air showers, or through scintillating plastics. Requirements vary, but the physics reach of experiments in all three frontiers can be extended through targeted improvements of photodetectors in following key areas:

- Improved time, spatial resolutions and lower background counts
- Robust operation under extreme working conditions such as high radiation environments, cryogenic temperatures, high pressures and high magnetic fields
- Signal collection over larger areas

Additionally, a substantial improvement in the cost-per-area coverage of photodetectors will have a positive impact on many current and next generation large scale high energy physics experiments such as (LHC, ATLAS and CMS @CERN, CLAS12 @Jefferson Lab, Mark-I @SLAC, LBNE/DUNE @Fermi Lab, PANDA @FAIR Germany, Super-K RICH and BELLE II @Japan, JUNO @China, etc.). The photodetectors for these experiments require high event rate, single photon capable light detection systems with sufficient granularity and position resolution. In particular, high performance photodetector devices integrated with MCPs can provide these essential functionalities for these various

*amane@anl.gov; Phone 1630-252-7014; Fax 1-630 252 1324; www. anl.gov

Hard X-Ray, Gamma-Ray, and Neutron Detector Physics XVIII, edited by Ralph B. James, Michael Fiederle, Arnold Burger, Larry Franks, Stephen A. Payne, Proc. of SPIE Vol. 9968, 99680C · © 2016 SPIE · CCC code: 0277-786X/16/$18 · doi: 10.1117/12.2237865

experiments. In the construction of MCP–photomultiplier tubes (PMTs), the classical dynode structure is replaced by MCPs allowing a compact device geometry. Most commercially available models are comparable to multianode-PMTs in terms of geometrical fill factor and granularity. The carefully crafted planes of small pores, which form the amplification sections of the complete MCP detector device, have been thoroughly characterized, and sophisticated simulation programs and an extensive literature exist to predict their performance.

MCP-photodetectors can provide excellent temporal resolution, spatial resolution, high gain, low background counts, compatibility with high magnetic fields, and long life [1-6]. These outstanding properties make MCP-detectors useful in a wide variety of applications including low-level signal detection, photodetection [1-8], gas electron multipliers (GEM)[9], time-of-flight (ToF) mass spectrometry, molecular and atomic collision studies, electron microscopy [11-13], field emission displays [14, 15], and night vision goggles and binoculars [16-18, 21] as well as emerging applications such as medical imaging (PET scanners) [19], homeland security (scanners for shipping containers and trucks).

1.2 MCP Working Mode

MCPs are two dimensional arrays of microscopic channels (diameter d=10-40μm, length l=0.5-5 mm) that each act as an independent electron multiplier. The basic operation of an MCP is as follows**:** a negative bias potential is applied between the input and output electrodes to generate a uniform electric field along the pores of the MCP. An incident electron striking on a pore wall near the input face of MCP and will induce the emission of secondary electrons from the pore surface. These secondary electrons will be accelerated further along the pore by the bias potential, ultimately resulting in their collision with the pore wall. These also produce secondary electrons, resulting in an electron avalanche inside the pore and the emission of a cloud of electrons from the output of the pore. Because the millions of pores each operate independently, the MCP is image-preserving. The amplification gain depends on the applied bias voltage, MCP pore size, l/d ratio and open area ratio. At typical high voltage of ~1kV, the gain per MCP is in the range of 10^3-10^6. The generation of secondary electrons is based on the incident electron energy, angle of incidence, and the secondary electron emission yield (SEY= δ) of the emission surface. The SEY is defined as the ratio of secondary electrons emitted to primary electrons incident on the surface. For practical reasons, MCPs are typically manufactured with intrinsic resistances in the range of 1MΩ-1GΩ, allowing the uniform electric filed and bias current to recharge electron depleted pores (post-avalanche) without drawing too much current. This prevents over-heating and eliminates the need for large high voltage power supplies [4, 20].

1.3 Conventional MCPs Creation Method

Conventional MCPs are fabricated using multi-fiber glass working techniques to draw, assemble, and etch an array of solid core fibers resulting in channels in a thin wafer of lead silicate glass [3, 4]. Although pore diameters as small as 6 microns have been achieved (Photonis Inc. or Hamamatsu Inc.), these channels are typically 10-40 microns in diameter, have an aspect ratio (α = L/D = pore length/pore diameter) of 50-100, and have an open area ratio (fraction of surface covered by pores) of 50-65%. Next, thermo-chemical processing such as H_2 firing is used to activate the channel walls for electron multiplication, and metal electrodes are evaporated onto both faces to provide electrical contact. Despite decades of refinement, the conventional process imposes serious limitations on MCP performance and size. One of the major drawbacks of conventional MCPs is that the electrical resistance and secondary electron emission (SEE) properties cannot be adjusted independently because both of these properties are imparted during the thermal activation step. In particular, lead glass MCPs have a relatively low SEY of ~2. Higher SEY values are desirable because they produce a higher gain at a given voltage, but unfortunately this SEY value is fixed during the hydrogen firing that is needed to impart electrical conductivity of the pores. Another shortcoming of conventional MCP's is the high manufacturing cost associated with the expensive lead silicate glass and the need to perform hydrogen firing, and this cost has prevented the scaling to larger areas. Last but not least, the scrubbing of conventional MCPs typically requires several weeks which adds to the cost. There have been several attempts to develop alternative MCP manufacturing strategies such as silicon micromachining [22], lithographic etching of anodic alumina [23], and thin film coatings on templates [24-26], but none of these technologies has succeeded in producing large area MCPs and viable commercial process and product.

1.4 ALD nanostructured functionalized MCPs Creation Method

In contrast to conventional MPCs comprised of leaded glass, the MCPs that are developed at Argonne with DOE LAPPD project [27] can be fabricated from nearly any substrate material with the appropriate pore structure because the electrical and SEE properties are imparted through functional nanostructured thin film coatings using ALD methods [27-

33]. For instance, starting with low cost large area borosilicate glass micro capillary arrays (MCAs) developed by Incom Inc., the electrical conductivity can be applied in one ALD coating, and SEE property can be applied with a second ALD coating. The uniqueness of ALD method compare to other thin film deposition techniques is, it utilizes the alternating exposures of reactive precursor vapors and a solid surface to deposit materials in an atomic layer-by-layer fashion. The ALD surface reactions are self-limiting because once the reactive surface sites are completely consumed, the ALD reactions terminate. The self-limiting surface chemistry, combined with gaseous diffusion of the precursor vapors, enables complex non-planar substrates, including MCPs with micron-scale, high aspect ratio pores and a high surface area, to be coated precisely, uniformly and conformally. In ALD, the surface reactions are performed sequentially, so that the two precursors are never mixed in the gas phase. This separation of the two reactants eliminates possible gas phase reactions that can form particles that could deposit on the surface to produce granular films. Moreover, the broad range of ALD precursors available which allows nearly wide range of nanostructure materials to be synthesized by ALD including metals, oxides, nitrides, fluorides, sulfides, and their composites [34-36]. All these attributes are what make ALD scheme so attractive for various type MCPs fabrication.

2. ALD FUNCTIONALISED BOROSILICATE MICROCAPILARY SUBSTRATES

ALD MCPs are based on a thin film nanostructure functionalization scheme where a borosilicate micro-capillary array can function as a template and the resistive and secondary emissive layers are deposited sequentially using ALD processes. This strategy results in an extremely robust device at reduced cost, and allows very large MCPs (20cmx20cm) to be produced with various pore sizes and MCP shapes. Evaporation of 150nm NiCr electrodes on both sides completes the MCP fabrication process. The resistance of MCPs fabricated can range from <1 MΩ to >1 GΩ, and either Al_2O_3 or MgO have been used as the high secondary emission coefficient electron multiplication layers [28,34,37].

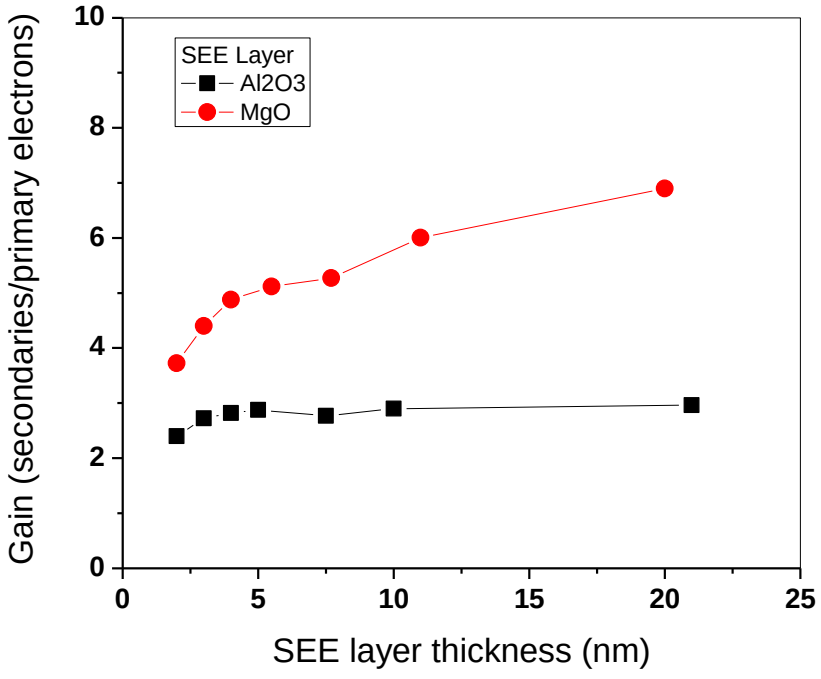

Figure 1. Secondary electron yield vs. film thickness for ALD MgO and Al_2O_3 [37].

For example of an ALD process, consider the deposition of MgO [38], an excellent secondary electron emitter [37] onto the borosilicate surface of a glass capillary array. In the first step, the borosilicate surface is exposed to bis-cyclopentadienyl magnesium ($MgCp_2$) vapor causing a reaction between the Mg compound and the hydroxyl (OH) groups on the glass and resulting in a monolayer of chemically-bound Mg-Cp species. These Mg-Cp surface species are inert towards additional $Mg(Cp)_2$ so that the entire surface of the high aspect ratio capillary pores becomes coated uniformly. Next, this surface is exposed to H_2O vapor and the Mg-Cp species are converted to MgO terminated with hydroxyls, allowing the ALD cycles ($MgCp_2/H_2O$) to be repeated to grow the MgO film to any desired thickness [34]. In contrast to this, instead of MgO if we integrate Gd_2O_3 layer by ALD using tris-methylcyclopentadienyl gadolinium $Gd(CpCH_3)_3$-H_2O precursors the same MCP can be used directly for thermal neutron detection [39].

Figure 1 demonstrate the maximum secondary electron yield vs. film thickness for ALD grown MgO and Al_2O_3 measured in ultra-high vacuum apparatus using a modified Low Energy Electron Diffraction (LEED) module for SEY measurements [37]. From Figure 1, it is clear that MgO is a better secondary electron emitter than Al_2O_3. For Al_2O_3, an SEYof 2.9 is achieved at a film thickness of 50 Å. This corresponds to the maximum escape length for a secondary electron in this sample The SEY becomes saturated and remaining constant for thicker samples. For the MgO films in contrast, the SEY continues to increase with film thickness over the entire range of films, achieving a value of 6.9 for the 200 Å film. Thicker MgO samples could not be examined due to sample charging. This charging occurs in thicker samples because of the increased distance electrons must travel from the conductive substrate to the origin of the secondary electron.

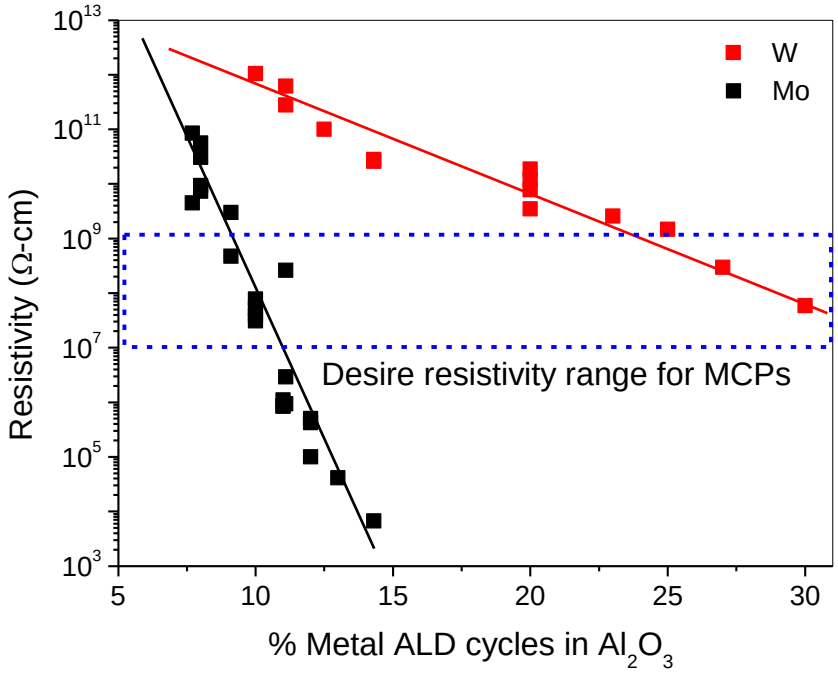

Figure 2. Resistivity of the Argonne ALD tunable resistance coatings (M:Al_2O_3; were M=Mo or W) used for functionalizing glass micro capillary arrays to produce MCPs versus the number of metal cycles.

In addition to ALD of simple binary compounds such as MgO or Al_2O_3, the more complex tunable resistance nanocomposite coatings can be synthesized by blending, at the atomic scale, insulating (e.g. Al_2O_3) and conducting (e.g. W) materials in the appropriate ratio to produce a composite film (e.g. W:Al_2O_3). The composition, and hence resistivity, of the film is dictated by the ratio of insulating and conducting components in the nanocomposite film. This ratio can be controlled to achieve a target resistivity by adjusting the relative number of ALD cycles performed to deposit the insulating and conducting components which is termed the precursor ratio. The resistivity of the nanocomposite M:Al_2O_3

(where M = W or Mo) can be tuned over many orders of magnitude by adjusting the metal to oxide ALD precursor cycles ratio (shown in Figure 2). Details about the ALD M:Al_2O_3 nanocomposite growth can be found in [34, 40, 41]. The resistivity of the molybdenum containing nanocomposite films has an exponential slope versus the metal cycle percentage twice that of the tungsten films because the amount of Mo deposited in a single Mo ALD cycle is approximately twice that of the W ALD [40]. This control in resistivity with ALD process parameters method can easily adapted to produce the MCPs with varying resistance that can be used in either cryogenic, ambient temperature, or high temperature applications. The highlighted dotted blue box in Figure 2 indicates the range of desirable resistivity values for most MCP applications. However, the MCP resistance can vary strongly with temperature, and this effect must be accounted for when the MCP is produced. Consequently the temperature coefficient of the resistance has been studied in detail and has been found to vary with composition as shown in Figure 3 for Mo:Al_2O_3 nanocomposites. These temperature coefficient of the resistance values are comparable to those of commercial MCPs. It is clear that depending on the target MCP operating condition (room, low or high temperature) we can tune the MCP resistance separately without affecting SEE properties by adjusting the ALD process parameters.

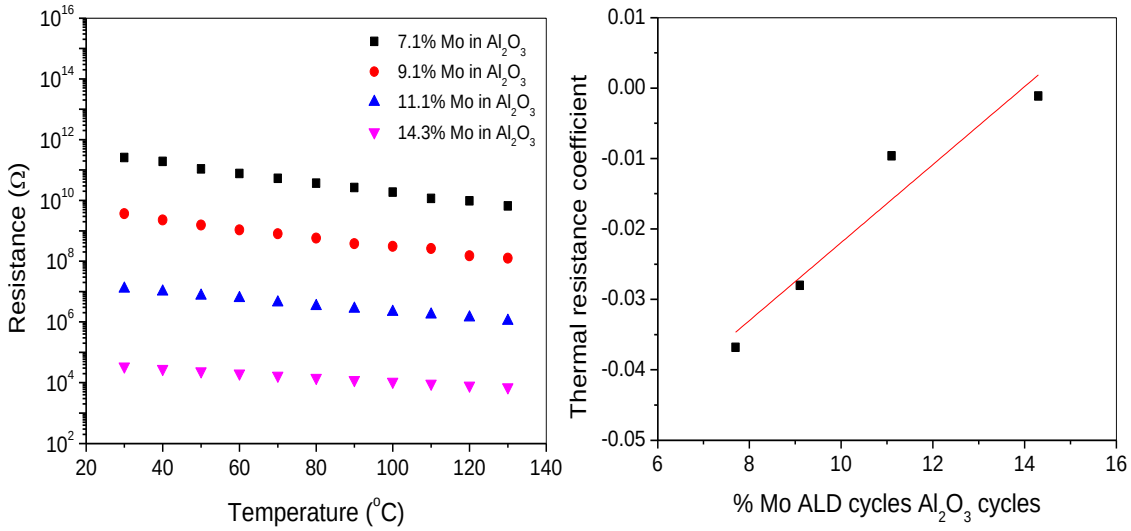

Figure 3. Resistance vs. temperature of ALD tunable resistance coatings (Mo:Al_2O_3) for various %Mo ALD cycles in Al_2O_3. Thermal coefficient of resistance was extracted from the temperature–resistance data for each composition in the left graph.

ALD W:Al_2O_3 nanocomposites were prepared using three different compositions: process-1 (medium %W) process-2 (high % of W), and process-3 (low % of W). The resistivity vs. temperature were measured for these films and are shown in Figure 4. For example, with process 2 it can be seen that at low temperature MCP operating conditions the resistance increased 2-3 order of magnitude or decreased 2-3 orders of magnitude (for process 1) in case of high temperature MCP operation from its room temperature resistance. This change in R needs to be accounted for during the ALD processing so that when the MCP is operated at the desired temperature stable operation is achieved and thermal runaway is avoided. Considering the data in Figure 4, the ALD process-3 MCPs can be used for high temperature (350-450K) operation whereas the ALD process-2 MCPs can be used for low temperature (150-200K) MCP operation. The ALD process-1 MCPs can be used around room temperature (273-325K).

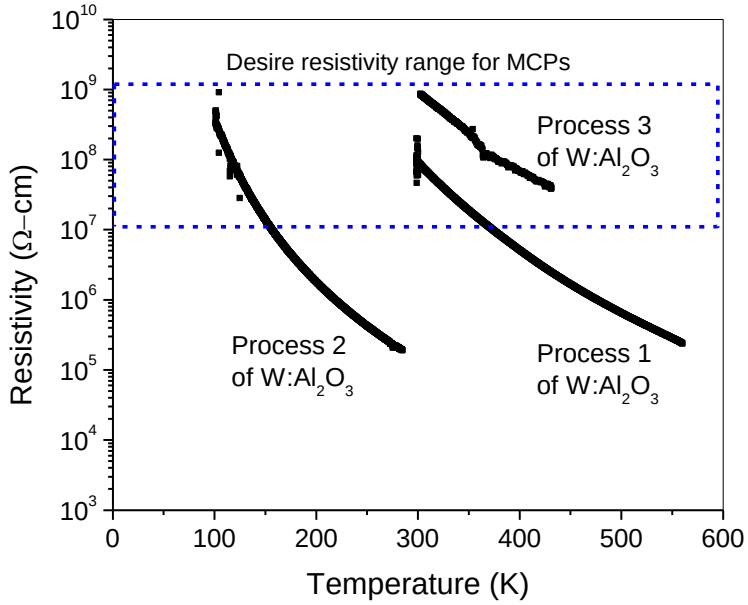

Figure 4. Resistivity vs. temperature of ALD nanocomposite resistance coatings of W:Al_2O_3 prepared using three different W compositions.

3. ALD MCPs PERFORMANCE

Initial ALD process development and MCP testing was performed on 33 mm substrates [32, 33] that showed many of the performance characteristics are typical of conventional MCPs. However, the background rates were found to be lower than conventional MCPs because the borosilicate glass contains less naturally occurring radioactive material compared to standard MCP glass formulations. We have also found that in pre-conditioning steps on borosilicate ALD MCPs, the gain can rise by an order of magnitude after a vacuum bake and then remain stable [32] during prolonged operation up to 7 C cm^{-2}. Most recently Incom's 2nd generation borosilicate glass substrate has been implemented with higher resiliency, larger pore open area ratios and better chemical compatibility with ALD coatings and subsequent photocathode depositions.

Further ALD processes were optimized to get uniform thin film deposition across the large area MCPs which is one of the challenging substrate for any thin film deposition process. For example, one (20cm x 20cm) MCP substrate with 65% open area ratio, and aspect ratio of 60 will have a surface area equivalent to ~100 x 300mm Si wafers. The photograph of the received Incom's MCA substrates (white) and after ALD MCP (black) are shown in Figure 5. By developing novel ALD hardware and processes, we have achieved uniform (<10%) depositions of both SEE and resistive layers across the 12" diameter MCP substrate [41]. With our best optimized ALD process condition now we can produce the 20cm x 20cm MCP in a few hours which is on par with the timing requirement for conventional equivalent batch processing of wafers in commercial ALD systems used in semiconductor manufacturing. Figure 6 displays the ellipsometric measured thickness and index of refraction (n) of one of the optimized (Resistive + SEE) layer stacks on Si(100) witness coupons positioned beneath the MCP(s) in the custom ALD reaction chamber. The ALD layers were highly uniformly over the 12" diameter of the MCP substrate. A growth per cycle of 1.7Å˚/cycle for one of the best known ALD process of W:Al_2O_3 nanocomposite and 1.3Å/cycle (100 cycles) for Al_2O_3 was measured. The refractive index is also highly uniform across the reactor indicating a uniform composition of the ALD films, and this has been verified using XPS and XRF measurements. Thickness values for both the resistive and SEE layer inside the MCP pores have been measured using cross-section SEM and TEM analysis and are within 5% of the thickness values measured by ellipsometry on witness coupons. This agreement lends confidence to using is the convenient and non-destructive ellipsometric measurements on witness coupons to gauge the thickness of the coatings inside of the MCP pores.

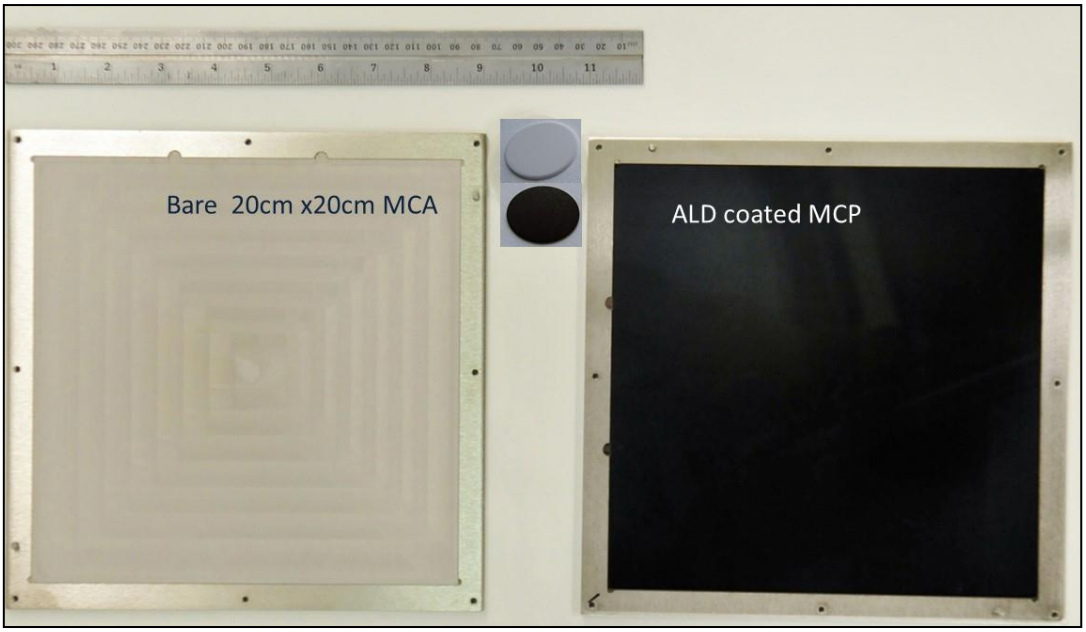

Figure 5. Photograph of Incom's bare 20cm x 20cm MCA (white) and ALD MCP 20cm x 20cm MCPs (black) with 33mm circular MCP inserted for comparison.

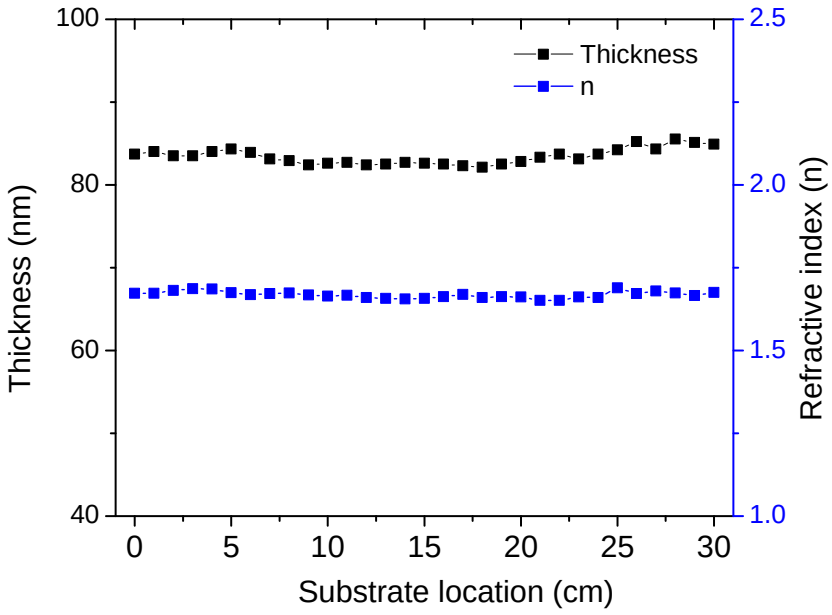

Figure 6. Film thickness and index of refraction measured by ellipsometry on witness Si coupons placed underneath MCP in 300mm reaction chamber for deposition of resistive layer (W:Al_2O_3) + SEE layer (Al_2O_3).

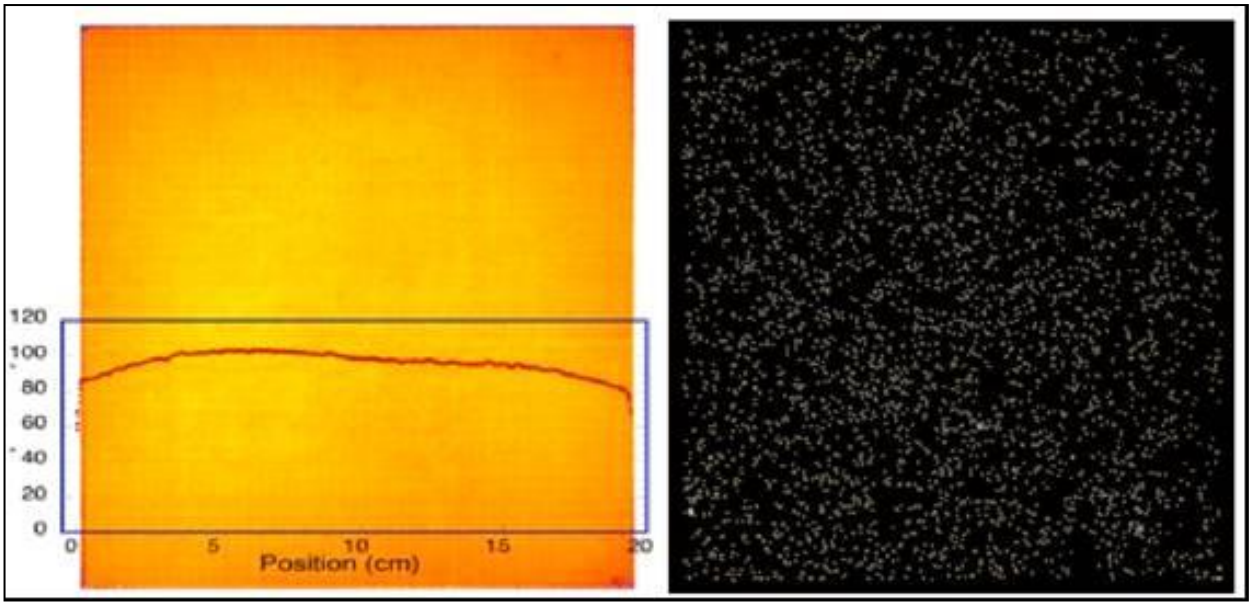

Figure 7. Average gain image map for 20cm x 20cm ALD MCP pair, pore size=20µm, L/d=60:1, ~7x10^6 gain with <15% variation (left image). A 300 sec background count image of ALD MCP pair. In general background counts are very low (0.028 sec^{-1} cm^{-2}) due to the absence of lead and reduced amounts of ^{40}K in the borosilicate glass (right image).

Tests with 33mm round format ALD MCPs on borosilicate substrates have established that the gain, pulse amplitude distribution, and MCP resistance are comparable to conventional MCPs [28-32]. Similar tests on large area (20cm x 20cm) MCPs have been done, using the standard format of 20 µm pores, 60:1 L/d, and an 8° pore bias angle [33]. The gains with the (20cm x 20cm) ALD MCP pairs with Al_2O_3 SEE layer can reach 10^7 or greater. With the large area format there are often problems with the spatial uniformity of the operating characteristics due to intrinsic variations in the multiplication process or simply the physical flatness of the MCPs. Both of these issues have been addressed and good performance data can be achieved. A gain map image containing > 10^8 events (Fig. 7 left image) shows the gain uniformity over the entire area is < 15%. Image quality tests were performed at the Berkeley Space Sciences Laboratory using the (20cm x 20cm) detector with 3 MCPs in a stack with a cross delay line readout. The background rate for borosilicate ALD MCPs is low (<0.07 events cm^{-2} s^{-1}) compared to conventional MCPs and is due to low intrinsic radioactivity in the glass. In large size formats, particulates and surface defects can cause local field emission (hot spots). However, we have been able to measure the background rate for (20cm x 20cm) MCPs that do have some debris, but show little or no signs of hot spot activity. In such MCPs we can see that the background rate (Fig.3 right image) can be very low, about 0.028 events cm^{-2} sec^{-1} for the general 400 cm^2 area, excluding 2 or 3 "warm spots". This level is comparable with the expected rate due to cosmic ray muon events and is as low as can be envisioned without precautions to shield the detector from external radiation.

Considering the excellent performance achieved by ALD nanostructured functionalized MCPs now we routinely create the ALD MCPs in a wide range pore size (6-40microm), shapes (squares, circles, trapezoidal, curved), aspect ratio of 20-600) and actual size from 1cm^2 -400cm^2. These MCPs have been integrated into sealed photodetectors with or without photocathode and their performance has been systematically evaluated [27, 29-33,42,]. Figure 8 shows a photographs of various ALD MCPs. The successful attempt also made to make sealed photodetectors in various sizes and shapes with ALD-MCPs in a collaboration with UCB, UoC, ANL HEP and Incom Inc. (shown in Figure 9). These ALD MCP photodetectors shows excellent stable long life performance in terms of gain (>10^7)/pair, timing (20-40ps) and spatial resolution (100µm), with low background and very short (2-3days) [29-33] scrubbing time compare to several weeks for commercial MCPs. We think this remarkable development for next generation MCPs.

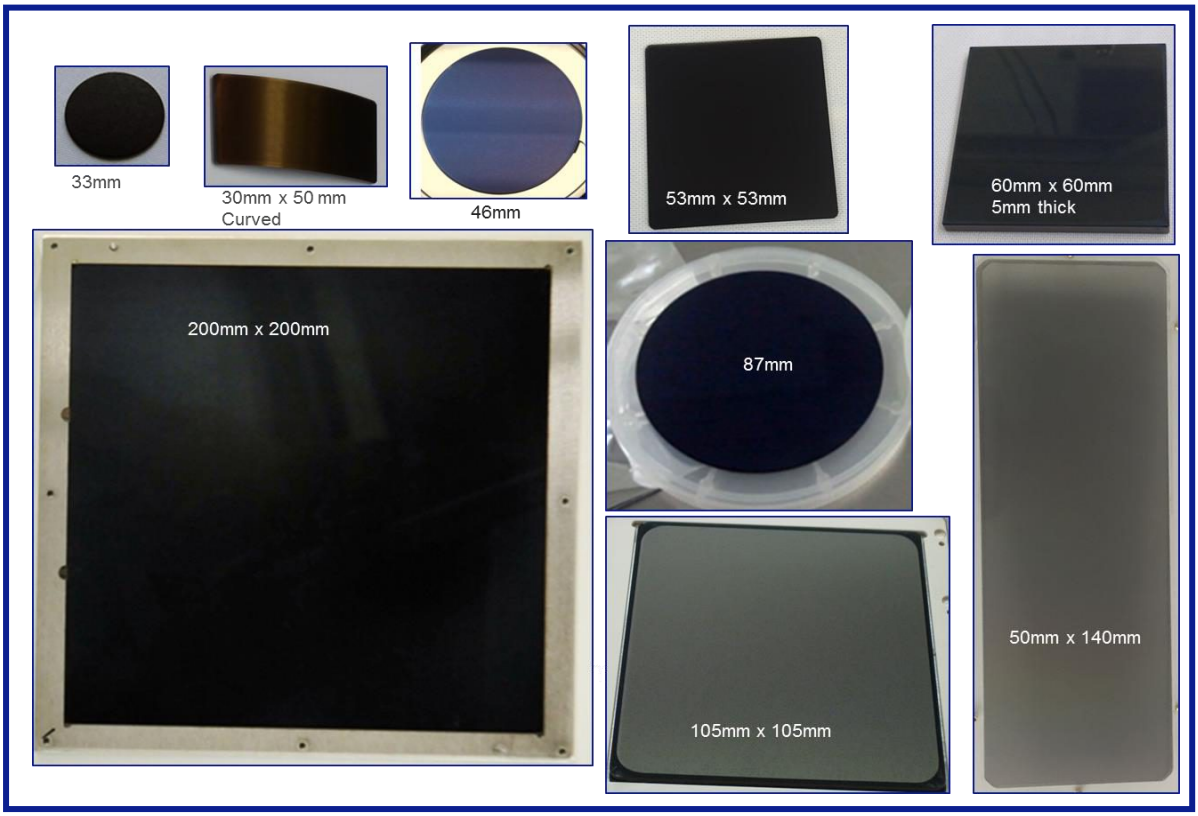

Figure 8. Photographs of various types of MCPs made using ALD nanostructure thin film functionalization

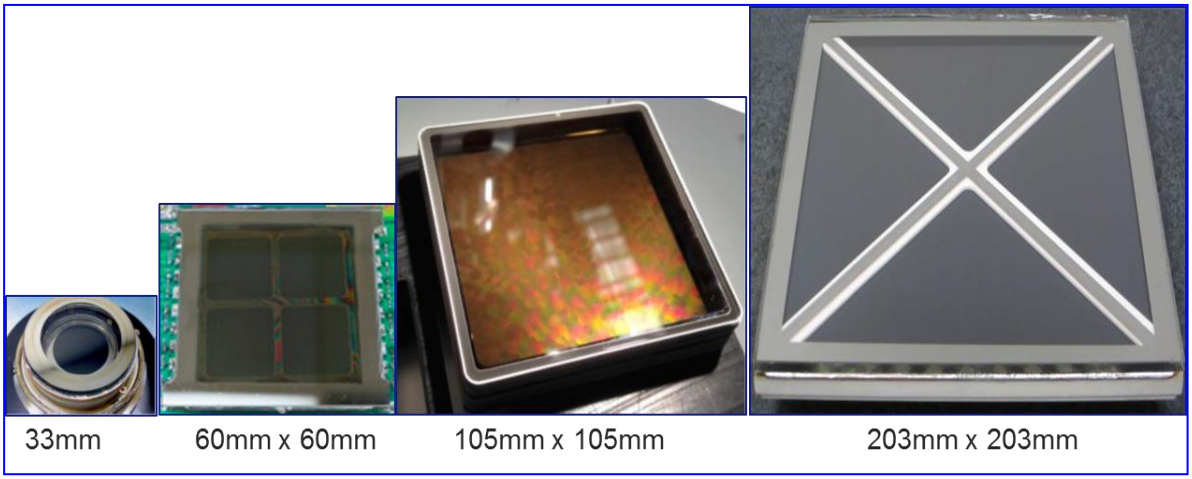

Figure 9. Photographs of various photodetectors that have been fabricated using ALD-MCPs [27, 29-33, 42]

4. SUMMARY

We have demonstrated a innovative process flow to fabricate various size and shape large area MCPs. To accomplished this we have developed M:Al_2O_3 (where M= Mo or W) nanocomposite coatings by ALD consisting of conducting, metallic nanoparticles embedded in an amorphous dielectric matrix. These ALD resistive layers shows conformal and uniform coating along the MCP pores and excellent reproducibility across multiple substrates and multiple batches. The characteristics of the resistive and SEE layers were tuned by adjusting the ALD process parameters such as temperature, composition, and precursor chemistry. MCP parameters such as SEY, thermal resistance coefficient and the desired application oriented resistance of the MCPs can be adjusted by ALD process parameters. Fully functionalized MCPs up to (20cm x 20cm) in size have been fabricated using this method, displaying good resistance stability, repeatable performance, high and uniform gain (>10^7 for pair) and 3-4 times lower background signals than commercial MCPs which are generally available in small form factor. ALD MCPs are used in many detectors and tested thoroughly. With this success we have now transferred the ALD MCP technology to Incom Inc. MA for commercialization.

5. ACKNOWLEDGEMENTS

This work was supported by the U.S. Department of Energy, Office of Science, Office of Basic Energy Sciences and Office of High Energy Physics under contract DE-AC02-06CH11357 as part of the Large Area Picosecond Photodetector (LAPPD) project. The views, opinions, and/or findings contained in this article/presentation are those of the author/presenter and should not be interpreted as representing the official views or policies, either expressed or implied, of the Defense Advanced Research Projects Agency or the Department of Defense.

6. REFERENCES

[1] Delendik, K.; Emeliantchik, I.; Litomin, A.; Rumyantsev, V.; Voitik, O., Nucl Phys B-Proc Sup, (2003) 125, 394.
[2] Siegmund, O. H. W.; Tremsin, A. S.; Vallerga, J. V.; Beetz, C. P.; Boerstler, R. W.; Winn, D., X-Ray and Gamma-Ray Instrumentation for Astronomy Xi, (2000) 4140, 188.
[3] Siegmund, O. H. W.; Tremsin, A. S.; Vallerga, J. V.; Beetz, C. P.; Boerstler, R. W.; Yang, J.; Winn, D., X-Ray and Gamma-Ray Instrumentation for Astronomy Xii, (2002) 4497, 139.
[4] Wiza, J. L., Nucl. Instrum. Methods, (1979) 162, 587.
[5] Wiza, J. L.; Henkel, P. R.; Roy, R. L., B Am Phys Soc, (1977) 22, 94.
[6] Seitz. B., Britting A., Cowie E., Eyrich W., Hoek M., Keri T., Lehmann A., Montgomery R., Uhlig F., Proc. SPIE, (2011) 37, 796
[7] Barnyakov, A. Y.; Barnyakov, M. Y.; Barutkin, V. V.; Bobrovnikov, V. S.; Buzykaev, A. R.; Gulevich, V. V.; Kononov, S. A.; Kravchenko, E. A.; Onuchin, A. P.; Tsigankov, D. A., Nucl Instrum Meth A, (2007) 572, 404.
[8] Inami K., Physics Procedia (2012) 37, 683
[9] Rispoli R., Proc. of SPIE Vol. 8450 84505L-1
[10] Czasch, A.; Dangendorf, V.; Milnes, J.; Schossler, S.; Lauck, R.; Spillmann, U.; Howorth, J.; Jagutzki, O., Advanced Photon Counting Techniques Ii, (2007) 6771, W7710.
[11] Dolenec, R.; Chagani, H.; Korpar, S.; Krizan, P.; Pestotnik, R.; Stanovnik, A.; Verheyden, R., 2009 IEEE Nuclear Science Symposium Conference Record, (2009) (1-5), 1558.
[12] Zuleta, I. A.; Yoon, O. K.; Robbins, M. D.; Barbula, G.; Zare, R. N., Abstr. Pap. Am. Chem. S, (2006) 231,
[13] Tremsin, A. S.; McPhate, J. B.; Steuwer, A.; Kockelmann, W.; Paradowska, A. M.; Kelleher, J. F.; Vallerga, J. V.; Siegmund, O. H. W.; Feller, W. B., Strain, (2012) 48, 296.
[14] Tremsin, A. S.; McPhate, J. B.; Vallerga, J. V.; Siegmund, O. H. W.; Feller, W. B.; Lehmann, E.; Butler, L. G.; Dawson, M., Nucl. Instrum. Meth A, (2011) 652, 400.
[15] Yu, S. G.; Whikun, Y. K.; Jeong, T.; Lee, J.; Heo, J.; Lee, C. S.; Jeon, D.; Kim, J. M., Journal of Vacuum Science & Technology a-Vacuum Surfaces and Films, (2002) 20, 950.
[16] Yi, W. K.; Jeong, T.; Jin, S. W.; Yu, S. G.; Lee, J.; Kim, J. M., Rev. Sci. Instrum., (2000) 71, 4165.

[17] Hadjar, O., Micro- and Nanotechnology Sensors, Systems, and Applications IV, SPIE. Proc. SPIE (2012) 8373, 837301,
[18] Siegmund, O.H.W. J.V. Vallerga, A. Tremsin, J. McPhate, B. Welsh, Advanced Maui Optical and Space Surveillance Technologies Conference Proceedings (2011) pp. E77.
[19] H. Kim H, Frisch H, Chen C-T, Genat J.-F., Tang F., Moses W. W., Choong W. S., Kao C.-M., Nuclear Instruments & Methods in Physics Research A. (2010) 622(3), 628.
[20] https://www.hamamatsu.com/resources/pdf/etd/PMT_handbook_v3aE.pdf
[21] Glesener, J.; Estrera, J., Optical Components and Materials Vii, (2010) 7598.
[22] Smith, A. W.; Beetz, C. P.; Boerstler, R. W.; Winn, D. R.; Steinbeck, J. W., Image Intensifiers and Applications Ii, (2000) 4128, 14.
[23] Govyadinov, A., Emeliantchik, I., Kurilin, A., Nucl Instrum Meth A, (1998) 419, 667.
[24] Beaulieu, D. R.,Gorelikov, D., de Rouffignac, R., Saadatmand, K., Stenton, K., Sullivan, N., Tremsin, A. S., Nucl. Instrum. Meth. A, (2009) 607, 81.
[25] [31] Beaulieu, D. R., Gorelikov, D., Klotzsch, H.,de Rouffignac, P., Saadatmand, K., Stenton, K.,Sullivan, N., Tremsin, A. S., Nucl. Instrum. Meth A, (2011) 633, S59.
[26] Feller, W. B., White, P. L., White, P. B., Siegmund, O. H. W.; Martin, A. P.; Vallerga, J. V., Nucl. Instrum. Meth A, (2011) 652, 25.
[27] http://psec.uchicago.edu/
[28] Mane, A. U., Peng, Q.,Wetstein, M. J., Wagner, R. G., Frisch, H. J., Siegmund, O. H. W., Minot, M. J.; Adams, B. W., Chollet, M. C., Elam, J. W., Proc. SPIE, (2011) 37 8031.
[29] Siegmund, O., J.V. Vallerga, A.S. Tremsin, J. McPhate, X. Michalet, S. Weiss, H.J. Frisch, R.G. Wagner, A. Mane, J. Elam, G. Varner, Advanced Maui Optical and Space Surveillance Technologies Conference, (2012).
[30] Ertley C. D, Siegmund O. H. W., Jelinsky S. R., Tedesco J., Minot M. J., O'Mahony A., Craven C. A., Popecki M., Lyashenko A. V., Foley M. R., Proc. SPIE 9915, (2016) 99152G-1
[31] Siegmund, O.H.W., J.B. McPhate, S.R. Jelinsky, J.V. Vallerga, A.S. Tremsin, R. Hemphill, H.J. Frisch, R.G. Wagner, J. Elam, A. Mane, IEEE Transactions on Nuclear Science, (2013) 60(2), pp. 923-931.
[32] Siegmund, O., N. Richner G. Gunjala, J.B. McPhate, A.S. Tremsin, H.J. Frisch, J. Elam, A. Mane, R. Wagner, C.A. Craven, M.J. Minot, Proc. SPIE 8859, (2013) 88590Y.
[33] Siegmund, O., J. McPhate, A.S. Tremsin, J.V. Vallerga, H.J. Frisch, R.G. Wagner, A. Mane, J. Elam, G. Varner, Advanced Maui Optical and Space Surveillance Technologies Conference, (2013).
[34] Mane A. U.; Elam J. W., Chem. Vap. Deposition (2013) 19, 186
[35] George S. M., Chem. Rev., (2010) 110, 111.
[36] Mane A.U., Allen A.J., Kanjolia R. K., Elam J. W., J, Phys. Chem. C (2016) 120 (18), 9874
[37] Jokela, S. J.; Veryovkin, I. V.; Zinovev, A. V.; Elam, J. W.; Peng, Q.; Mane, A. U., Aip Conf Proc, (2011) 1336, 208.
[38] Burton, B. B.; Goldstein, D. N.; George, S. M., J, Phys. Chem. C, (2009) 113, 1939.
[39] Lu, N., Yang Y., Lv J., Pan J., Liang L., Wang X., Li Y., Physics Procedia, (2012) 26, 61
[40] Mane A.U., Tong W. M., Brodie A. D., McCord M. A., and Elam J. W., ECS Transactions, (2014) 64 (9) 3-14
[41] Elam J.W., Mane A.U., US Patents Number: 8,921,799 B2 and 9,105,379 B2.
[42] Ertley C. D, Siegmund O. H. W., Schwarz J., Mane A. U., Minot M. J. O'Mahony A., Craven C. A., Popecki M., Proc SPIE 9601, (2015), 96010S-1